Improved Gain of a Compact Slot Antenna using an FSS Reflector for GNSS L1/E1/B1/G1 Bands

Assia BOULARAS [1], Mustapha FLISSI [2], Khaled ROUABAH [3], Boualem HAMMACHE [4]

[1] Dept. of Electrical Systems Engineering, LIST Laboratory, M'hamed Bougara University, Boumerdes, Algeria
[2] ETA Laboratory, University Mohamed El-Bachir El-Ibrahimi of Bordj Bou Arreridj, Algeria
[3] Electronics Dept., University of M'sila, University Pole, Road Bordj Bou Arréridj, M'sila 28000, Algeria
[4] Electronics Department, University of Constantine 1, Algeria

a.boularas@univ-boumerdes.dz

Submitted June 9, 2024 / Accepted October 25, 2024 / Online first November 12, 2024

Abstract. *In this paper, a compact stepped slot antenna, for Global Navigation Satellite System (GNSS) applications, is proposed. The latter one, which operates in the frequency range from 1.49* GHz *to 1.66* GHz*, is designed to cover five GNSS bands namely GPS-L1, Galileo-E1, GLONASS-G1, BEIDOU-B1 and EGNOS-L1. The proposed composite design is carried out in three phases. Firstly, a compact slot antenna, having a size of 58.0 × 52.0 × 1.6 mm, is designed on FR4 substrate to generate the five GNSS bands. Secondly, a compact Frequency Selective Surface (FSS) reflector, with 18.0 × 18.0 × 1.6 mm unit size, is designed to produce a stop band response matching all these bands. Finally, a single layer FSS, consisting of 9 × 9 units, is combined with the optimized antenna to achieve a high-gain directional antenna structure. The final proposed combination has been investigated using the High Frequency Structure Simulator (HFSS) and validated by Computer Simulation Technology (CST) Microwave Studio. Besides, a prototype antenna is fabricated and validated by measurements. The measurement results, which illustrate a good agreement with those corresponding to the simulations, have shown that the proposed composite antenna exhibits a directional radiation pattern with a high peak gain of 7.3 dBi and a maximum gain improvement of 5.65 dBi at 1.57 GHz. Furthermore, it offers good radiation efficiency in the operating bands, which makes it a good candidate for multi-systems GNSS receivers, especially to reduce the different interferences by enhancing the antenna radiation characteristics.*

Keywords

FSS, GNSS, GPS, slot antenna, high gain antenna, multiband

1. Introduction

GNSS, including the Global Positioning System (GPS), plays a crucial role in delivering highly accurate positioning and essential services, such as navigation, timing, and mapping across various applications [1], [2]. Recent advancements in GNSS receivers involve the integration of measurements from multiple frequencies (MF) and multiple constellations (MC), which significantly enhance reliability and precision, even in environments with limited satellite visibility [3].

Despite these advancements, GNSS still faces several challenges, including multipath [4–6], various forms of interference [7], [8] and weak signal reception characterized by a low Signal-to-Noise Ratio (SNR) [9]. To address these issues, three primary approaches can be employed to enhance GNSS receiver performance, focusing on different technological aspects: antenna-based technology [10], [11], signal processing technology [12], [13], and measurement domain processing technology [14].

Focusing on antenna-based processing, the utilization of high-gain antennas can significantly enhance signal reception in areas where signals are weak. This improvement positively impacts performance, especially in the presence of multipath, interferences and low signal conditions [15]. In other words, high-gain antennas effectively reduce positioning errors associated with multipath effects and interferences within the GNSS receiver [16].

GNSS antennas are available in various configurations, including patch antennas, helical antennas, ceramic chip antennas, and various other designs [17]. Among these, planar antennas, such as slot and patch antennas, are the most commonly used in GNSS applications due to their low profile, compact size, and cost-effectiveness [18], [19]. However, planar antennas often have limitations, such as narrow bandwidth and lower gain. To tackle these challenges, planar antennas can be combined with FSS structures, which enhance their radiation characteristics by reflecting electromagnetic waves in specific frequency ranges [20–22].

Various GNSS antenna structures have been proposed in the literature to improve gain. For instance, in [23], a reconfigurable monopole loop antenna operating in the GPS L1 frequency band achieved a maximum gain of

DOI: 10.13164/re.2024.0733

about 4.2 dBi but suffered from low radiation efficiency due to the PIN diode losses. Another design presented in [24] achieved a peak gain of 4.69 dBi at 1.55 GHz frequency, although it exhibited a significantly lower gain of 0.68 dBi for large angles 85°. In [25], a cavity-backed magneto-electric dipole antenna tailored for GNSS applications was proposed. While this structure provides consistent gain and a stable radiation pattern, its performance within the desired frequency band is suboptimal, resulting in a simulated maximum gain of approximately 3.5 dBi for closely spaced antenna array elements in the GPS L1 band. In [26], a compact L1/L2 GPS antenna utilizing a meandered slot and high-dielectric substrate was developed. Though this structure reached a maximum simulated gain of 3.5 dBi on the GPS L1 band, it was limited by mutual coupling effects among closely spaced antenna elements. The authors in [27] proposed an antenna structure for GNSS applications composed of three stacked circular layers with a central feeding point. This design exhibited omnidirectional directivity and achieved a maximum gain of only 2.1 dBi, which is considered lower than those reported in the existing studies.

Several techniques have been proposed in the scientific literature to address the challenge of redirecting the backside radiation from antennas to the main lobe direction, thereby enhancing gain and directivity. Numerous studies have reported on antennas integrated with FSS reflectors within the context of GNSS radionavigation. For example, in [28], a circular patch antenna utilizing a Polarization Selective Surface (PSS) was developed to mitigate multipath interference in GPS receivers, achieving a peak gain of approximately 5 dBi. However, this design is constrained by its high complexity, leading to increased costs. In [29], a compact FSS reflector consisting of three metal strips connecting two metallic rectangles was proposed to enhance the gain of a monopole antenna, resulting in gain improvement of about 4 dBi. However, its limited directivity restricts its applicability across various applications. In [30], authors presented a U-shaped patch antenna combined with a single-layer FSS reflector aimed at enhancing both gain and directivity. This configuration demonstrates a favorable radiation pattern and high gain within the operating band. Nevertheless, the design does not adhere to the principle of maintaining an equal number of unit-cells on the X and Y axes, raising concerns regarding reliability of the results, particularly when alterations are made to the FSS reflector.

In this paper, we propose a compact stepped slot antenna designed for GNSS L1/E1/B1/G1 bands. The antenna structure features a stepped slot etched into the ground plane, measuring $58.0 \times 52.0 \times 1.6$ mm. In addition, an integrated single-layer FSS reflector is positioned beneath the antenna to improve its radiation characteristics. This proposed structure is designed and analyzed using HFSS and CST Microwave Studio. To validate the simulated results, the final design is fabricated and subjected to testing. The experimental outcomes demonstrate a good agreement between the measured and simulated radiation characteristics. Moreover, the proposed antenna, combined with the FSS reflector, exhibits a directional radiation pattern and achieves a gain improvement of 5.65 dBi at 1.57 GHz.

The rest of this paper is organized as follows: Section 2 describes the geometry and analysis corresponding to the proposed antenna alone and proposed FSS unit-cells. It also shows the proposed combined design as well as the CST and HFSS simulation results. In Sec. 3 and 4, the experimental results of the fabricated structure are compared with those reported in literature. Finally, we end with a conclusion.

2. Antenna Structure Design

This section outlines the innovative approaches taken in designing the antenna structure, emphasizing the integration of a compact slot antenna with FSS. The design principles and methodologies will be detailed, focusing on the unique attributes that enhance performance in terms of bandwidth and gain.

2.1 Principle of the Proposed Compact Slot Antenna

The proposed antenna design focuses on miniaturization and improved performance compared to previous works. This is achieved through the implementation of a specific stepped slot in the ground plane, based on a comprehensive literature review of slot antennas. Various methods exist for reducing antenna size, with the slot technique in the ground plane proving particularly effective. Building upon established techniques, the stepped slot integrates multiple slot configurations, allowing the current to take a longer path around the slots to reach the opposite edge, thereby reducing the antenna size and lowering the resonance frequency. In our work, a compact size and a resonance frequency of 1.58 GHz for GNSS applications are achieved by optimizing the dimensions of the stepped slot and the position of the microstrip line. The stepped slot serves multiple purposes, including:

- Reducing the antenna size by altering the current path and distribution.
- Creating a matching point at the desired frequencies.

The stepped slot is composed of several elementary slots, and their combination extends the current path in the ground plane, directly influencing the resonance frequency. The relationship between the resonance frequency and the length of the radiating slot L is established as follows:

$$L = \frac{\lambda}{4} \tag{1}$$

where λ is the wavelength at the target resonance frequency $f_0 = 1.57$ GHz. The proposed slot antenna is excited using an open-end microstrip line placed on top of the

substrate. The width of the microstrip line W is chosen to realize an impedance of 50 Ω, and can be calculated using the characteristic impedance equations given by [31]:

$$Z_0 = \begin{cases} \dfrac{60}{\sqrt{\varepsilon_{\text{eff}}}} \ln\left(\dfrac{8d}{W} + \dfrac{W}{4d}\right) & \text{for } \dfrac{W}{d} \le 1 \\ \dfrac{120\pi}{\sqrt{\varepsilon_{\text{eff}}}\left[\dfrac{W}{d} + 1.393 + 0.667\ln\left(\dfrac{W}{d} + 1.444\right)\right]} & \text{for } \dfrac{W}{d} \ge 1 \end{cases} \tag{2}$$

with

$$\varepsilon_{\text{eff}} = \frac{\varepsilon_r + 1}{2} + \frac{\varepsilon_r - 1}{2} \frac{1}{\sqrt{1 + \dfrac{12d}{W}}}. \tag{3}$$

Here, d represents the substrate thickness, and ε_r is the relative permittivity. The coupling resonator is modeled as a parallel RLC circuit, with the input impedance peaking at approximately 50 Ω at 1.58 GHz (see Fig. 1).

Figure 2 presents the equivalent circuit of the proposed antenna. In the model of Fig. 2, the impedance Z_a represents the equivalent circuit model of the antenna, where R is the resistor, L is the inductor, and C is the capacitor. The impedance Z_a is connected in parallel with the resonator, representing the operating band. To determine the values of the resonators (R, L, and C), it is crucial to calculate the bandwidth (BW) and quality factor (Q) of the parallel RLC resonators. BW is defined as the range where the real part of the impedance or resistance is equal to or greater than $R_{\max}/\sqrt{2}$.

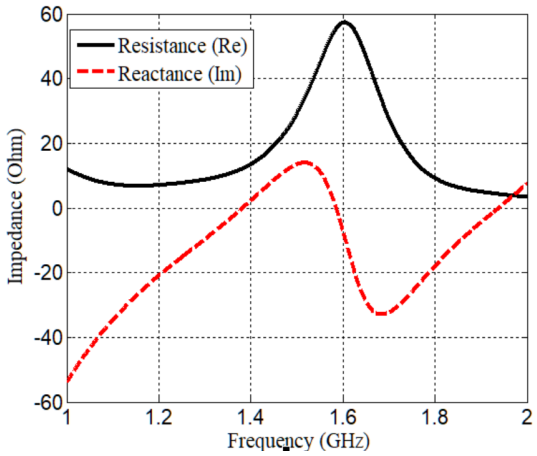

Fig. 1. Input impedance of proposed antenna.

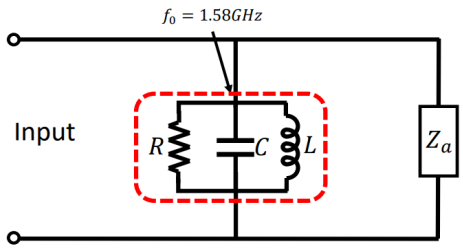

Fig. 2. Equivalent circuit of the proposed antenna.

The relationships of BW and Q at the resonant frequency, are determined by the following equations [31]:

$$f_0 = \frac{1}{2\pi\sqrt{LC}}, \tag{4}$$

$$Q = \frac{f_0}{\text{BW}}. \tag{5}$$

For a parallel RLC resonator:

$$Q = 2\pi f_0 RC. \tag{6}$$

Figure 3 shows the top and bottom views of the proposed slot antenna, of size 58.0 × 52.0 × 1.6 mm. As illustrated in this figure, the proposed antenna is designed on FR4 substrate with a dielectric constant of 4.3, a thickness of 1.6 mm, and loss tangent of 0.0025. The antenna is fed by a 50 Ω microstrip line with a width of W_f = 3 mm and a length of L_f = 38 mm. At the base of the antenna, a stepped slot is etched in the ground plane.

The reflection coefficient of the proposed antenna structure, calculated using both CST microwave studio and Ansoft HFSS, is illustrated in Fig. 4. It can be shown, from this figure, that for both CST and HFSS, the proposed antenna provides a frequency band corresponding to GPS (L1), Galileo (E1), GLONASS (G1), BeiDou (B1) and the European Geostationary Navigation Overlay Service (EGNOS) (L1). Furthermore, the impact of the SMA (Sub Miniature version A) connector on the reflection coefficient is clearly depicted in the same figure. Indeed, there is a negligible variation in the antenna's adaptation.

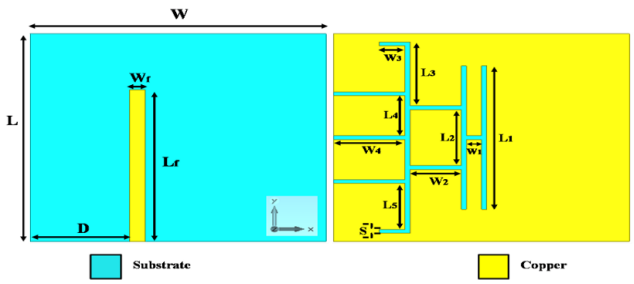

Fig. 3. Geometry of the proposed antenna element.

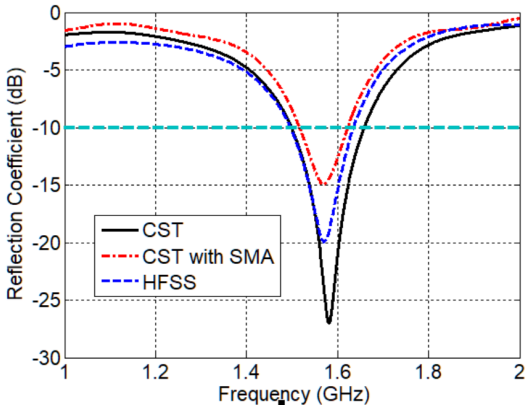

Fig. 4. Reflection coefficient of the proposed antenna simulated with CST Microwave Studio (without SMA connector), CST Microwave Studio (with SMA connector) and Ansoft HFSS.

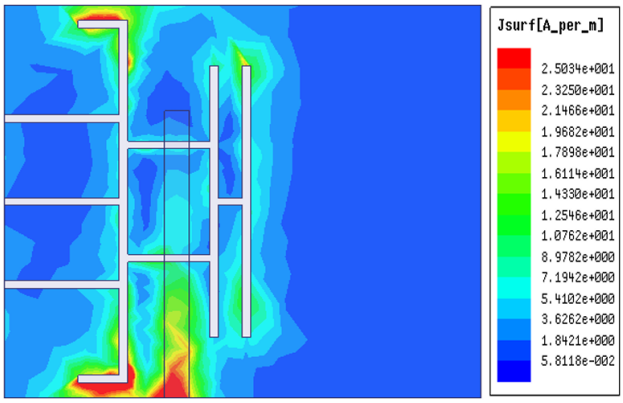

Fig. 5. Current distribution of the proposed antenna at 1.58 GHz.

Figure 5 shows the surface current distribution of the proposed antenna at a frequency 1.58 GHz. From this figure, it is obvious that the current concentration is focused around the edge of W_3.

A detailed parametric study was carried out to assess the impact of critical antenna parameters on overall performance, with particular emphasis on the width W_3 and the distance D. By systematically varying these parameters, the optimal design configuration was identified to meet key performance objectives, including impedance matching and bandwidth enhancement. First, all parameters were kept constant while W_3 was varied. Then, with all other parameters held constant, the parameter D was varied. The analysis below specifically examines how changes in W_3 and D influence the antenna's reflection coefficient (S11).

Figure 6 shows the influence of W_3 on the reflection coefficient (S11) of the proposed antenna. Here, W_3 is varied from 1 mm to 9 mm and all the other parameters are kept constant. As illustrated in this figure, the frequency band shifts toward lower frequencies when W_3 increases. The desired frequency band is therefore obtained by setting W_3 to 5 mm.

Figure 7 depicts the simulated reflection coefficient of the proposed antenna for different values of D, the distance

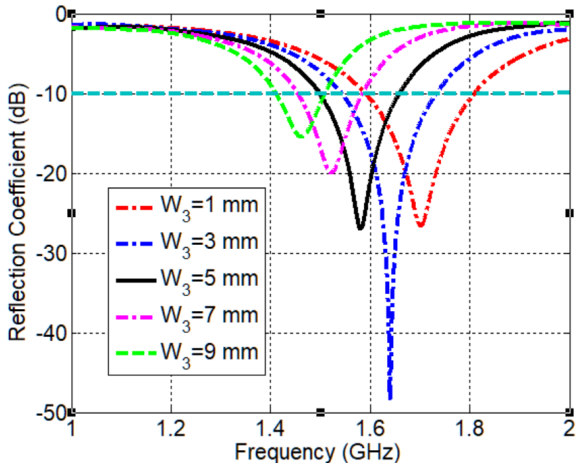

Fig. 6. Reflection coefficient of the proposed antenna for different values of W_3.

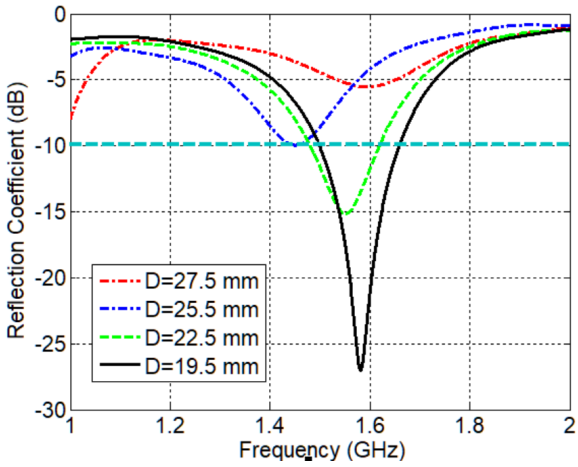

Fig. 7. Reflection coefficient of the proposed antenna for different values of D.

W	L	W_f	L_f	D	L_1	L_2
58	52	3	38	19.5	36	14
L_3	L_4, W_2	L_5	W_1	S	W_3	W_4
16	10	11.5	3	1	5	14

Tab. 1. Antenna structure parameters (units: mm).

between the feed line and the antenna's extremity. As illustrated in this figure, the best antenna adaptation occurs when D = 19.5 mm.

After the parametric study was conducted, the final dimensions of the proposed antenna are listed in Tab. 1.

2.2 FSS Unit-cell Design

Figure 8 illustrates the geometry of the proposed FSS unit-cell. The proposed unit-cell is fabricated on FR4 substrate with a dielectric constant of 4.3, a loss tangent of 0.0025 and a thickness of 1.6 mm. It consists of two elements: a square loop at the extremities and a metal square in the center of the structure. The total size of the FSS unit-cell is 18.0 × 18.0 × 1.6 mm.

In addition to the antenna optimization process described earlier, a comprehensive parametric study was conducted for the FSS unit-cell to optimize its performance.

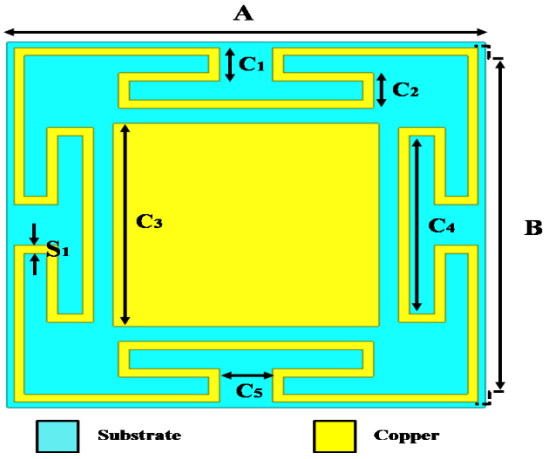

Fig. 8. Geometry of FSS unit-cell.

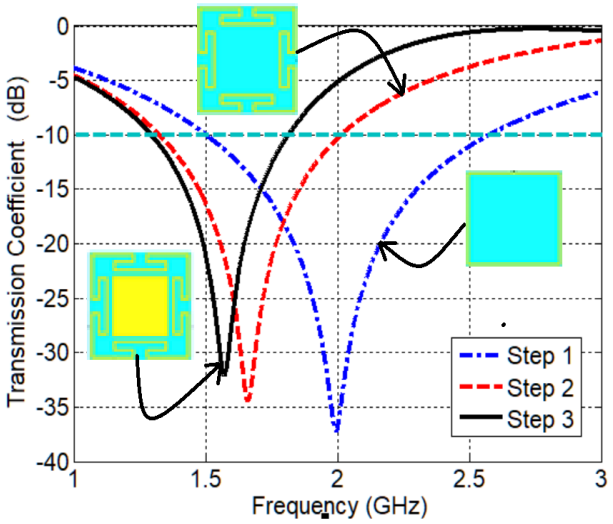

Fig. 9. Transmission coefficient of FSS unit-cell for different steps.

The optimization focused on key parameters such as the dimensions of the unit-cell, the slot width S_1 (C_1, C_2, C_3, C_4, C_5, and S_1), and the periodicity. Each parameter was systematically varied while keeping other parameters constant to assess its impact on the FSS's transmission characteristics.

Figure 9 shows the simulated transmission coefficient curves for each step in the design of the proposed FSS unit-cell. As shown in this figure, the first part of the FSS unit-cell consists of a large metal square loop element, designed to generate a stop-band response at 2 GHz.

The second part of the FSS unit-cell consists of a square metal loop, which resonates at 1.6 GHz. Finally, resonance at 1.58 GHz, corresponding to the L1/E1/G1/M1 bands is achieved by combining the square loop metal with the central square metal element of the unit-cell.

For instance, the slot width S_1 was varied to determine its influence on the resonance frequency and bandwidth. By evaluating the reflection coefficients at various frequencies, the optimal configurations were identified to achieve the desired band-stop response. Furthermore, the interaction between the FSS and the integrated antenna was considered during the optimization process to ensure improved overall performance, particularly in terms of impedance matching and gain enhancement. This systematic approach led to the final design parameters of the FSS unit-cell, which are crucial for the antenna-FSS integration. The final optimized parameters of the FSS unit-cell are given as follows: A = 18 mm, B = 17.5 mm, S_1 = 0.4 mm, C_1 = 1.65 mm, C_2 = 1.75 mm, C_3 = 10 mm, C_4 = 8.8 mm, C_5 = 2 mm.

Figure 10 illustrates the simulated S-parameters in dB of the FSS unit-cell, which resonates at 1.58 GHz, achieving a transmission coefficient S21 of –32 dB. The stop-band, characterized by an S21 below –10 dB, extends from 1.3 GHz to 1.8 GHz, effectively attenuating signals over a 500 MHz range. With an insertion loss of just 0.22 dB, the FSS operates as a reflector, directing desired signals

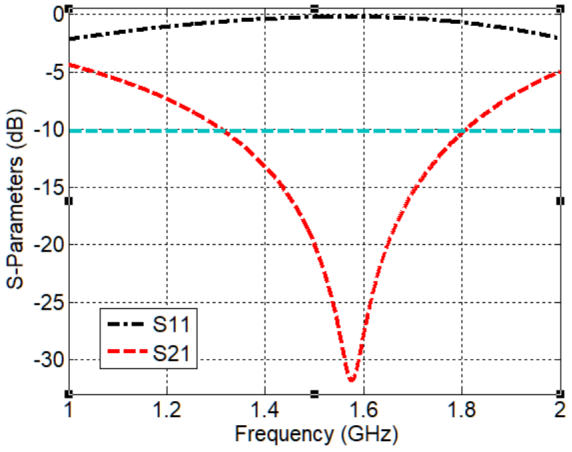

Fig. 10. Simulated S-parameters of the proposed FSS unit-cell.

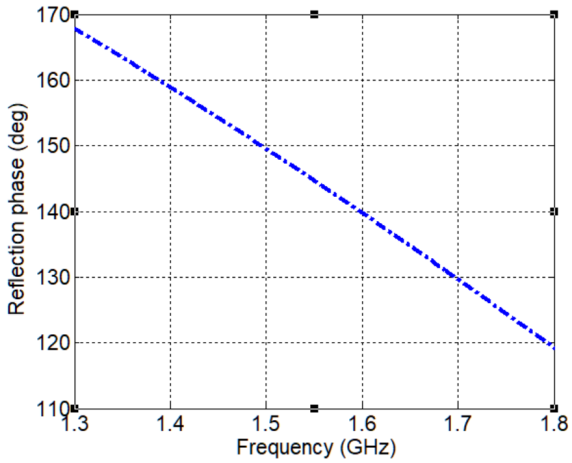

Fig. 11. Reflection phase of the proposed unit-cell.

within the stopband back toward the main lobe of the antenna, thereby optimizing performance within this frequency range.

The reflection phase of the proposed unit cell is illustrated in Fig. 11. Figure 11 demonstrates that the reflection phase decreases linearly across the entire operational bandwidth of the FSS unit cell. This linear decrease is beneficial for enhancing antenna gain, as it promotes constructive interference with backscattered waves from the antenna. By effectively managing the phase response, the FSS contributes to improved performance and efficiency of the antenna system, resulting in enhanced overall radiation characteristics.

2.3 Antenna Integration with FSS

The configuration of the proposed antenna combined with the FSS reflector is presented in Fig. 12. As illustrated in this figure, the FSS reflector consists of a single layer composed of an arrangement of 9 × 9 units along of the X–Y axes. It is installed below the proposed antenna at a distance of K, in order to enhance its radiation characteristics, in terms of gain, directivity, and radiation efficiency. The distance between the antenna and FSS reflector is calculated using (7) given as:

$$\varphi_{FSS} - 2\beta K = 2N\pi, N = 1, 2, 3, 4, 5. \quad (7)$$

φ_{FSS} is the FSS reflection phase, β is the propagation constant in open space, K is the distance between the antenna and FSS reflector [32].

Figure 13 shows the simulated reflection coefficient of the proposed antenna with and without FSS reflector. Both antenna structures have the same resonance frequency, which is equal to 1.58 GHz. The adaptation value is slightly different, estimated at –27.1 dB for the antenna alone and –37.3 dB for the antenna with FSS.

The bandwidth of the antenna with the FSS reflector changed slightly compared to that of the antenna alone, with a frequency range extending from 1.57 GHz to 1.66 GHz.

To show the effect of FSS reflector on the radiation characteristics, such as realized gain and radiation efficiency, a comparison was made between the antenna with FSS reflector and the antenna alone. The results of simulated realized gain are shown in Fig. 14.

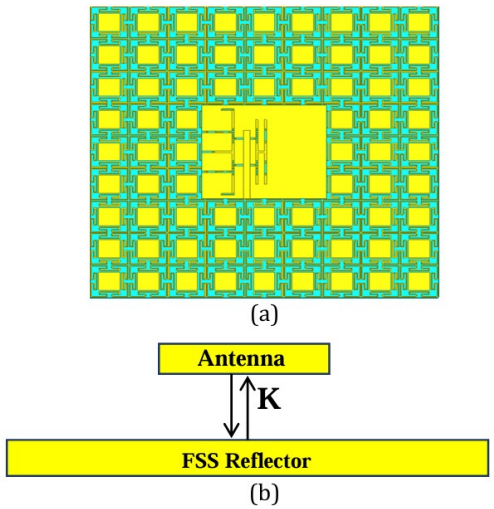

Fig. 12. Antenna integration with FSS reflector: (a) Top view. (b) Side view.

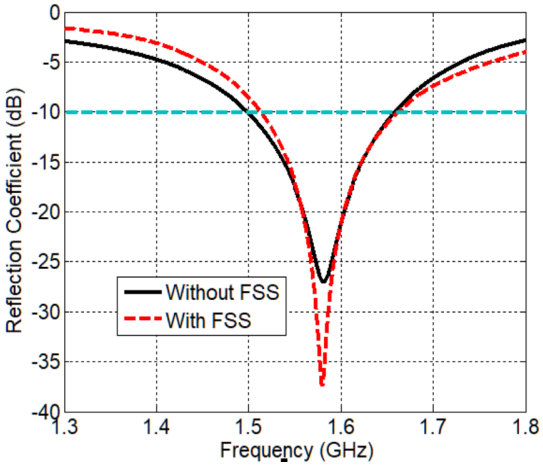

Fig. 13. Simulated reflection coefficient of the proposed antenna with and without FSS.

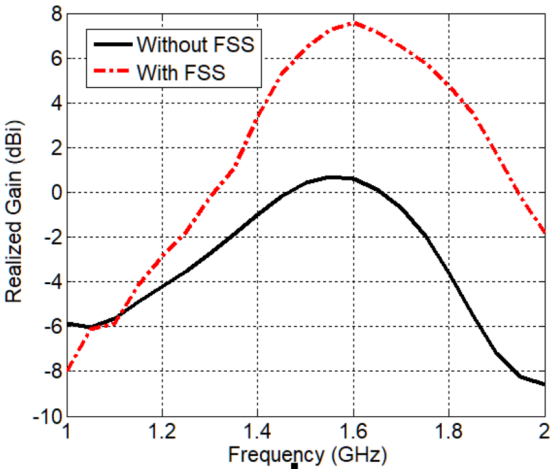

Fig. 14. Realized gain of the proposed antenna with and without FSS reflector.

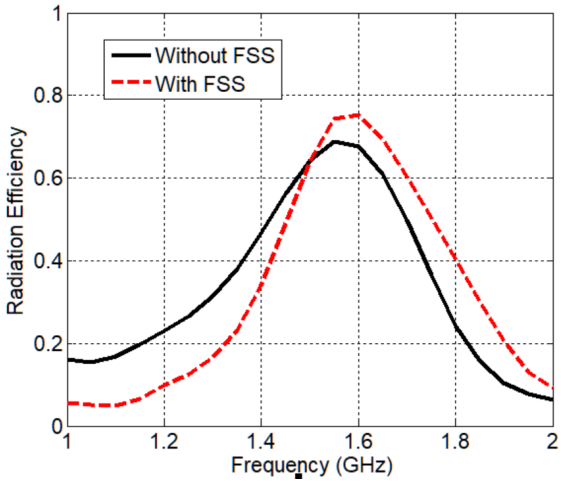

Fig. 15. Radiation efficiency of the proposed antenna with and without FSS reflector.

As illustrated in Fig. 14, the variation of the realized gain as a function of frequency for the antenna alone shows a positive gain in the operating band located between 1.46 GHz and 1.66 GHz, with a maximum gain of 0.8 dBi at 1.58 GHz frequency. However, the variation of the realized gain for the antenna with FSS reflector indicates an improvement in the realized gain along the L1/E1/G1/M1 bands. At this point, the maximum gain is 7.57 dBi at 1.58 GHz frequency which corresponds to an improvement of 6.77 dB.

Figure 15 shows the simulated radiation efficiency of the proposed antenna with and without FSS reflector. As shown in this figure, the maximum radiation efficiency of the antenna alone is 0.68, while that of the antenna with FSS is 0.76 at the operating frequency of 1.58 GHz.

In what follows, a parametric study will be conducted to determine the effect of the FSS reflector on the antenna alone. The first parametric study involves modifying the distance between the antenna and the FSS reflector. Figure 16 presents the simulated reflection coefficient, realized gain and radiation efficiency of the proposed antenna with the FSS reflector for different values of K.

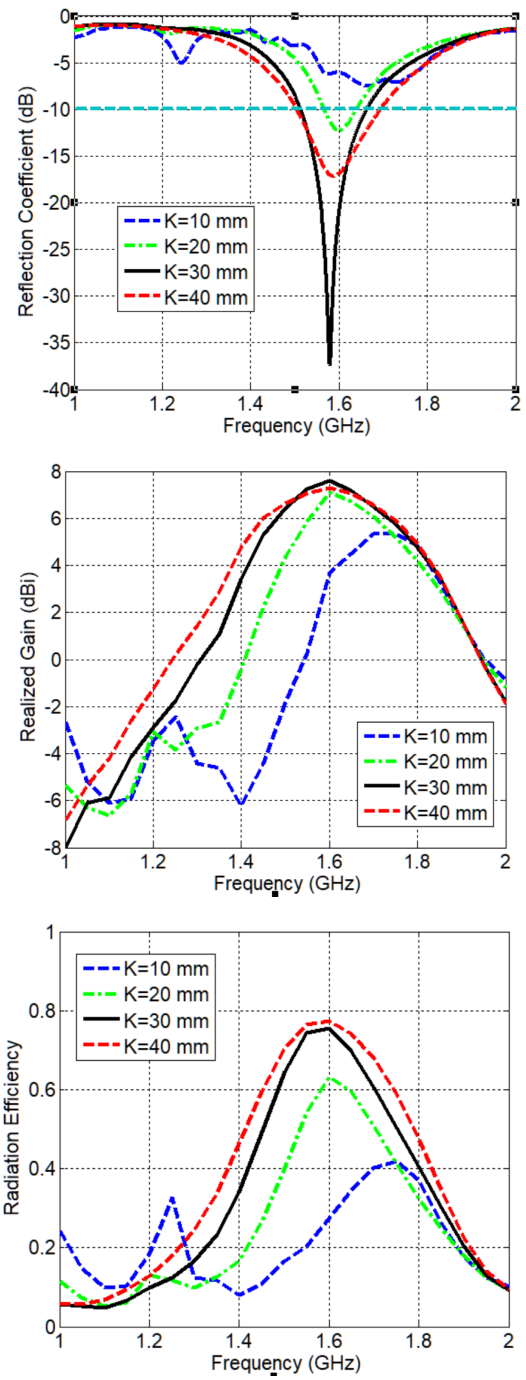

Fig. 16. Simulated results of the proposed antenna with FSS reflector for different values of *K*. Top: Reflection coefficient; Middle: Realized gain; Bottom: Radiation efficiency.

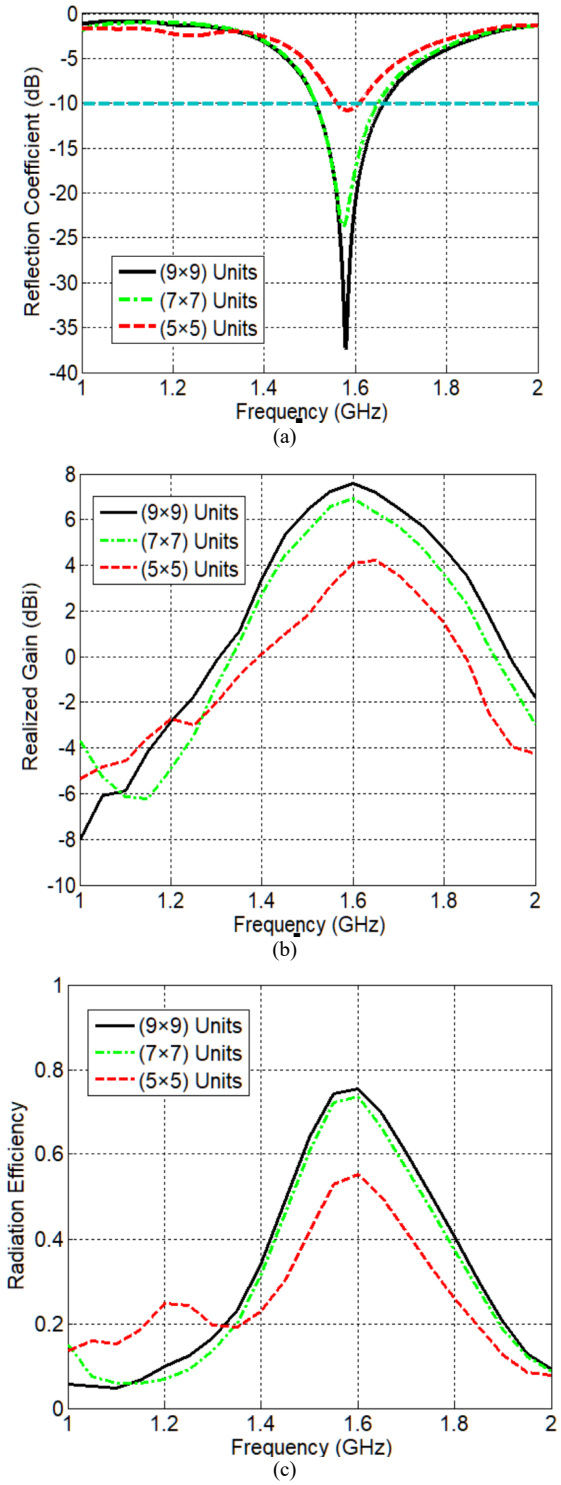

Fig. 17. Simulated results of the proposed antenna for different sizes of FSS reflector: (a) Reflection coefficients; (b) Realized gain; (c) Radiation efficiency.

As shown in Fig. 16, the optimal value of *K*, corresponding to the best antenna impedance matching, is chosen to be $K = 30$. At this value, the reflection coefficient is equal to –37 dB, and the maximum gain level reaches 7.57 dBi. Furthermore, at this optimal value, the antenna achieves a maximum radiation efficiency of 0.76 at the desired frequency.

The second parametric study is carried out as a function of the size of the FSS reflector. The results, in terms of reflection coefficient, realized gain and radiation efficiency are presented in Fig. 17. From this figure, it is clear that the size of the FSS reflector plays a vital role in increasing the performances of the proposed antenna. In fact, the antenna matching improves as the number of unit-cells increases from 5×5 units to 9×9 units. Furthermore, a considerable improvement in realized gain and radiation efficiency is observed when the FSS reflector size is increased to 9×9 units.

3. Measurement Results and Discussion

Figure 18 depicts the photograph of the fabricated prototype of the proposed antenna structure. As this figure shows, the proposed antenna alone, constructed from an FR4 substrate, has dimensions of $58.0 \times 52.0 \times 1.6$ mm. The FSS reflector, consists of 9×9 units, each having a size of $18.0 \times 18.0 \times 1.6$ mm. The measured S-parameters for the proposed prototype were obtained using the Agilent 8722ES network analyzer. Furthermore, the radiation patterns and gain were measured in an anechoic chamber for the E-plane (YZ) and H-plane (XZ) at 1.57 GHz.

Figure 19 represents a comparison between the measured and simulated reflection coefficients of the proposed antenna, both with and without FSS reflector. As shown in this figure, the measured frequency band of the antenna alone ranges from 1.50 GHz to 1.62 GHz with a resonance frequency located at 1.57 GHz. For the fabricated structure, consisting of the antenna integrated with FSS, it has an operating band between 1.52 GHz to 1.64 GHz with a resonance frequency of 1.58 GHz. It is evident from this figure, that the operating bands in both cases (with and without FSS) show good agreement with the simulated results.

As exposed by these results, incorporating the FSS reflector into our antenna design has led to a slight shift in the operating band. However, both configurations remain well-suited for GNSS applications. The primary reason for integrating the FSS is to enhance specific radiation characteristics of the antenna, such as directivity and gain, especially in challenging environments. Although the slight degradation in the reflection coefficient may appear concerning, this trade-off can be justified by the observed improvements in other performance metrics. Figure 20 presents the measured and simulated radiation patterns of the proposed antenna with and without FSS reflector at 1.57 GHz.

As illustrated in Fig. 20, the antenna without the FSS reflector exhibits an omnidirectional radiation pattern in the

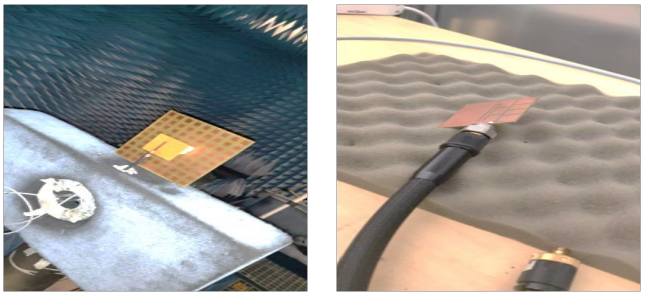

Fig. 18. Photography of the fabricated antenna.

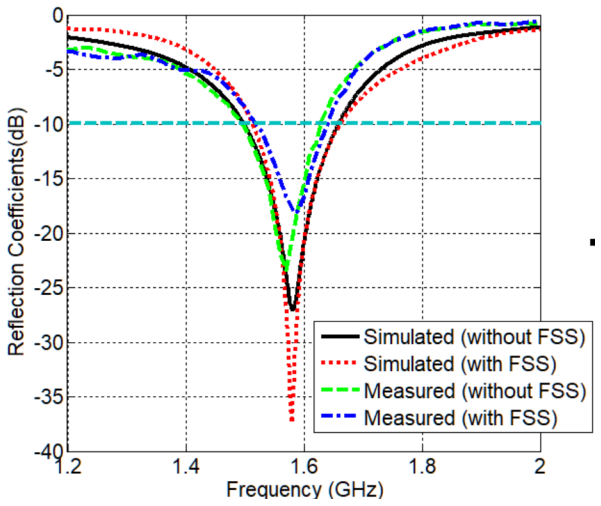

Fig. 19. Measured and simulated reflection coefficients of the antenna with and without FSS.

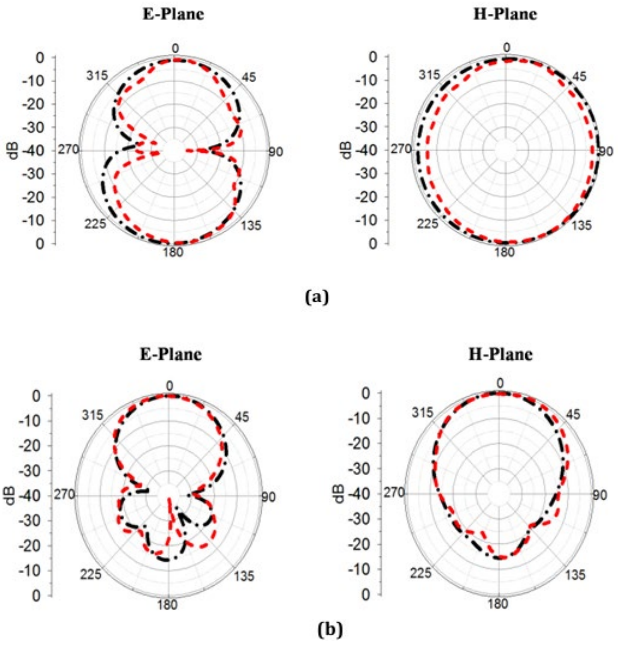

Fig. 20. Measured and simulated radiation patterns of the proposed antenna with and without FSS for $f = 1.57$ GHz: (a) without FSS reflector; (b) with FSS reflector.

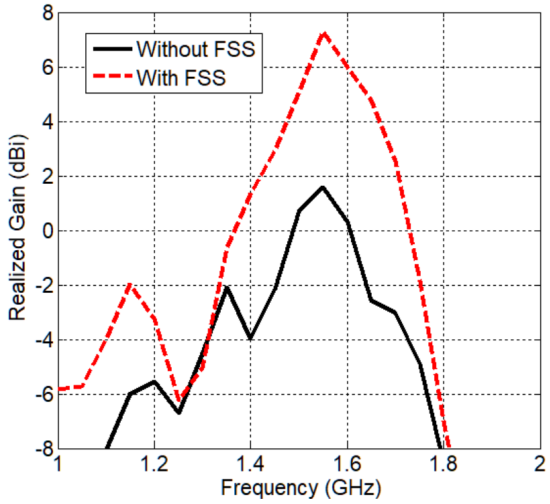

Fig. 21. Measured realized gain of proposed antenna.

Ref.	Dimension (mm)	Bandwidth (GHz)	Realized gain (dBi)
[28]	150 × 150 × 14	1.54–1.61	5
[33]	127.5 × 127.5 × 1.6	1.5831–1.5893	2.31
[26]	117.2 × 117.2 × 13	1.54–1.59	3.5
[34]	300 × 300 × 10	1.55–1.59	5
This work	**162 × 162 × 33.2**	**1.52–1.64**	**7.3**

Tab. 2. Comparison between the proposed antenna and the most relevant of those reported in the literature.

H-plane and bidirectional pattern in E-plane. In contrast, a directional radiation pattern is exhibited by the proposed antenna combined with the FSS reflector in both planes. Besides, the comparison between the simulated and measured results, regarding the radiation patterns of both structures, reveals good agreement.

Figure 21 illustrates the measured realized gain of the proposed antenna with and without FSS reflector. According to this figure, the measured realized gain of the proposed antenna without the FSS reflector reaches a peak of 1.65 dBi at a frequency of 1.57 dBi, while the maximum value for the proposed antenna combined with the FSS reflector is 7.3 dBi. The measured realized gain shows thus an improvement of 5.65 dBi when comparing the antenna with the FSS reflector to the antenna alone.

4. Comparison Results

The proposed compact stepped slot antenna is compared to the most relevant designs reported in the scientific literature. The results, in terms of antenna dimensions, bandwidth, and realized gain, are given in Tab. 2. As shown in this table, the proposed antenna has an acceptable compact size of 162 × 162 × 33.2 mm and offers a larger bandwidth compared to the structures presented in other works. In addition, a high realized gain is achieved by the proposed antenna, demonstrating that its overall performance is superior compared to that of previously reported designs in the scientific literature.

5. Conclusion

In this paper, a new, simple, compact stepped slot antenna integrated with a novel FSS reflector has been designed, simulated, and validated through measurements. The proposed antenna structure, which has a compact size of 162 × 162 × 33.2 mm, demonstrates good performance for radionavigation applications operating in the frequency range from 1.52 GHz and 1.64 GHz covering the L1/E1/G1/M1 bands. The obtained results show a high agreement between simulations and measurements in terms of reflection coefficient, realized gain and radiation pattern. The integration of the FSS reflector improves the gain by approximately 5.65 dBi, reaching a maximum value of 7.3 dBi at 1.57 GHz. Moreover, compared to the antenna alone, the radiation pattern of the proposed antenna combined with the FSS reflector has become more directional, with reduced backlobe levels.

References

[1] CATA, M. Exactly positioning determination using global navigation satellite system (GNSS). *Analele Ştiinţifice ale Universităţii (Ovidius) Constanţa, Ser.: Matematică,* 2003, vol. 11, no. 2, p. 43–50. [Online] Available at: http://eudml.org/doc/125833

[2] CHEN, X., PARINI, C. G., COLLINS, B., et al. *Antennas for Global Navigation Satellite Systems.* Wiley, 2012. DOI: 10.1002/9781119969518

[3] CHEBIR, S., AIDEL, S., ROUABAH, K., et al. GNSS signals acquisition and tracking in unfavorable environment. *Radioengineering*, 2018, vol. 27, no. 2, p. 557–571. DOI: 10.13164/re.2018.0557

[4] ROUABAH, K., ATTIA, S., FLISSI, M., et al. Efficient technique for DLL S-curve side zero-crossings cancellation in global positioning system/Galileo receiver. *IET Signal Processing*, 2019, vol. 13, no. 3, p. 338–347. DOI: 10.1049/iet-spr.2018.5379

[5] HUSSAIN, A., AHMED, A., MAGSI, H., et al. Adaptive GNSS receiver design for highly dynamic multipath environments. *IEEE Access*, 2020, vol. 8, p. 172481–172497. DOI: 10.1109/ACCESS.2020.3024890

[6] ROUABAH, K., CHIKOUCHE, D., BOUTTOUT, F., et al. GPS/Galileo multipath mitigation using the first side peak of double delta correlator. *Wireless Personal Communications,* 2011, vol. 60, no. 2, p. 321–333. DOI: 10.1007/s11277-010-9946-2

[7] GAO, G. X., SGAMMINI, M., LU, M., et al. Protecting GNSS receivers from jamming and interference. *Proceedings of IEEE*, 2016, vol. 104, no. 6, p. 1327–1338. DOI: 10.1109/JPROC.2016.2525938

[8] FLISSI, M., ROUABAH, K., ATTIA, S., et al. Consistent BCS modulated signals for GNSS applications. *IET Signal Processing*, 2017, vol. 11, no. 4, p. 415–421. DOI: 10.1049/iet-spr.2016.0200

[9] STRODE, P. R. R., GROVES, P. D. GNSS multipath detection using three-frequency signal-to-noise measurements. *GPS Solution*, 2016, vol. 20, p. 399–412. DOI: 10.1007/s10291-015-0449-1

[10] SKLAR, J. R. Interference mitigation approaches for the global positioning system. *Lincoln Laboratory Journal*, 2003, vol. 14, no. 2, p. 167–179.

[11] FANTE, R., KUNYSZ, W., RAO, B. R. *GPS/GNSS Antennas*. Artech House, 2013. ISBN: 9781596931503

[12] FERNANDEZ-PRADES, C., ARRIBAS, J., CLOSAS, P. Robust GNSS receivers by array signal processing: Theory and implementation. *Proceedings of IEEE*, 2016, vol. 104, no. 6, p. 1207–1220. DOI: 10.1109/JPROC.2016.2532963

[13] DARDARI, D., FELLETTI, E., LUISE, M. (Eds.) *Satellite and Terrestrial Radio Positioning Techniques: A Signal Processing Perspective.* Academic Press, 2011. DOI: 10.1016/C2009-0-61856-0

[14] BORIO, D., GIOIA, C. GNSS interference mitigation: A measurement and position domain assessment. *Navigation: Journal of the Institute of Navigation,* 2021, vol. 68, no. 1, p. 93–114. DOI: 10.1002/navi.391

[15] VOLAKIS, J. L., O'BRIEN, A. J., CHEN, C. C. Small and adaptive antennas and arrays for GNSS applications. *Proceedings*

of IEEE, 2016, vol. 104, no. 6, p. 1221–1232. DOI: 10.1109/JPROC.2016.2528165

[16] MAQSOOD, M., GAO, S., BROWN, T. W. C., et al. A compact multipath mitigating ground plane for multiband GNSS antennas. *IEEE Transactions of. Antennas and Propagation*, 2013, vol. 61, no. 5, p. 2775–2782. DOI: 10.1109/TAP.2013.2243692

[17] AMAMI, M. Testing patch, helix and vertical dipole GPS antennas with/without choke ring frame. *International Journal for Research in Applied Science and Engineering Technology*, 2022, vol. 10, no. 2, p. 933–938. DOI: 10.22214/ijraset.2022.40396

[18] CHEN, Z. N., CHIA, M. Y. W. *Broadband Planar Antennas: Design and Applications.* Wiley, 2006. DOI: 10.1002/0470871768

[19] GARCIA GAMEZ, L. Analysis and design of compact antennas in cavity based on metasurfaces for multiband GNSS applications. *Theses.* Universite Rennes 1, 2020.

[20] BOULARAS, A., ROUABAH, K., FLISSI, M. Miniaturized self-complementary frequency selective surface for GNSS applications. In *IEEE International Symposium on Antennas and Propagation and USNC-URSI Radio Science Meeting (APS/URSI)*. Singapore, 2021, p. 1707–1708. DOI: 10.1109/APS/URSI47566.2021.9704590

[21] ANWAR, R. S., MAO, L., NING, H. Frequency selective surfaces: A review. *Applied Sciences*, 2018, vol. 8, no. 9, p. 1–46. DOI: 10.3390/app8091689

[22] PANWAR, R., LEE, J. R. Progress in frequency selective surface-based smart electromagnetic structures: A critical review. *Aerospace Science and Technology*, 2017, vol. 66, p. 216–234. DOI: 10.1016/j.ast.2017.03.006

[23] FAKHARIAN, M. M., REZAEI, P., OROUJI, A. A. Polarization and radiation pattern reconfigurability of a planar monopole-fed loop antenna for GPS application. *Radioengineering*, 2016, vol. 25, no. 4, p. 680–686. DOI: 10.13164/re.2016.0680

[24] SUN, Y. X., LEUNG, K. W., LU, K. Broadbeam cross-dipole antenna for GPS applications. *IEEE Transactions of Antennas and Propagation*, 2017, vol. 65, no. 10, p. 5605–5610. DOI: 10.1109/TAP.2017.2742585

[25] CAUSSE, A., RODRIGUEZ, K., BERNARD, L., et al. Compact bandwidth enhanced cavity-backed magneto-electric dipole antenna with outer Γ-shaped probe for GNSS bands. *Sensors*, 2021, vol. 21, no. 11, p. 1–11. DOI: 10.3390/s21113599

[26] CHEN, M., CHEN, C. C. A compact dual-band GPS antenna design. *IEEE Antennas and Wireless Propagation Letters*, 2013, vol. 12, p. 245–248. DOI: 10.1109/LAWP.2013.2247972

[27] AKMAL, M., ALIELDIN, A., ELDAMAK, A. R. A high-power sandwiched omnidirectional circularly polarized antenna for GNSS systems. *IEEE Access*, 2023, vol. 11, p. 31167–31176. DOI: 10.1109/ACCESS.2023.3262236

[28] KHOSRAVI, F., MOGHADAS, H., MOUSAVI, P. A GNSS antenna with a polarization selective surface for the mitigation of low-angle multipath interference. *IEEE Transactions of Antennas and Propagation*, 2015, vol. 63, no. 12, p. 5287–5295. DOI: 10.1109/TAP.2015.2491323

[29] TAHIR, F. A., ARSHAD, T., ULLAH, S., et al. A novel FSS for gain enhancement of printed antennas in UWB frequency spectrum. *Microwave and Optical Technology Letters*, 2017, vol. 59, no. 10, p. 2698–2704. DOI: 10.1002/mop.30789

[30] MONDAL, R., REDDY, P. S., SARKAR, D. C., et al. Compact ultra-wideband antenna: Improvement of gain and FBR across the entire bandwidth using FSS. *IET Microwaves, Antennas and Propagation*, 2020, vol. 14, no. 1, p. 66–74. DOI: 10.1049/iet-map.2019.0536

[31] POZAR, D. M. *Microwave Engineering*. 4th ed. Wiley, 2011. P. 147–148. ISBN: 978-0-470-63155-3

[32] KUMAR, A., DE, A., JAIN, R. K. Gain enhancement using modified circular loop FSS loaded with slot antenna for sub-6 GHz 5G application. *Progress in Electromagnetics Research Letters*, 2021, vol. 98, p. 41–48. DOI: 10.2528/PIERL21031108

[33] SUPRIYA, A. S., RAJENDRAN, J. A low cost tri-band microstrip patch antenna for GPS application. In *Progress in Electromagnetics Research Symposium-Fall (PIERS-FALL)*. Singapore, 2017, p. 60–65. DOI: 10.1109/PIERS-FALL.2017.8293111

[34] BAGGEN, R., MARTINEZ-VAZQUEZ, M., LEISS, J., et al. Low profile GALILEO antenna using EBG technology. *IEEE Transactions of Antennas and Propagation*, 2008, vol. 56, no. 3, p. 667–674. DOI: 10.1109/TAP.2008.916927

About the Authors...

Assia BOULARAS is a Doctoral student in Telecommunications Systems at M'Hamed Bougara Boumerdes University. In 2019 she received her Master degree in Telecommunication Systems from the University of Bordj Bou Arréridj Algeria. Since 2020, she has been affiliated with LIST Laboratory, University M'Hamed Bougara Boumerdes. Her research interests are: frequency selective surfaces (FSS), GNSS application, compact slot antenna, circular polarized antenna and reconfigurable antenna.

Mustapha FLISSI was born in Setif, Algeria in 1970. He received the B.S. and M.S. degrees in Electronics Engineering from the University of Farhat Abbas, Setif, Algeria, in 1995. He obtained his Magister degree in Communications in 2001 from the University of Farhat Abbas, Setif, Algeria, and the doctorate degree in Electronics from the University of M'sila, Algeria, in 2015. He joined the Electronics Department, University of Ziyani Achour, Djelfa, Algeria, as an Assistant Professor in 2002. Then, in 2005 he joined the Electronics Department of the University of Mohamed Bachir El-Ibrahimi, Bordj Bou Arreridj, Algeria, also as an Assistant Professor. Since 2014, he works as a Lecturer at the same department. He is a Member of ETA Laboratory of the same department since 2015. His research interests include satellite navigation, signal structure design and signal processing.

Khaled ROUABAH received his engineering degree in Electronics from the University of Farhat Abbas, Setif, Algeria, in 1999. He obtained his Master's degree in Telecommunications and Networking in 2001 from the Higher Institute of Aeronautics and Space, Toulouse, France, his Magister degree in Communications and his Ph.D. degree in Electronics Engineering from the University of Farhat Abbas, Setif, Algeria, in 2005 and 2010, respectively. In 2013, he obtained his HDR degree in Electronics in Mohamed BOUDIAF University of Msila. Between July 2018 and October 2022, he worked as a Professor in the Department of Electronics at Mohamed EL Bachir El Ibrahimi University, Bordj Bou Arreridj. He is currently holding the same position at the Electronics Department of Mohamed BOUDIAF University of Msila. His research interests include communication signals, geolocation, parallel processing, pattern recognition, hardware implementation,

signal structure design, mobile computing and telecommunications networks.

Boualem HAMMACHE received his PhD degree in Telecommunications from the University of Constantine 1, in 2021 and his Master degree in Networks and Telecommunication Technologies from the University of Bordj Bou Arréridj Algeria, in 2013. He is with the Department of Electronics, University of Constantine 1, Algeria. His research interests include microstrip antennas, UWB antennas, notched-band UWB antennas, slot antennas, reconfigurable UWB antennas, circular polarized slot antennas, and frequency selective surfaces (FSS).